ACS APPLIED NANO MATERIALS

www.acsanm.org Article

Piezo/Triboelectric Nanogenerator from Lithium-Modified Zinc Titanium Oxide Nanofibers to Monitor Contact in Sports

Nishat Kumar Das, Om Priya Nanda, and Sushmee Badhulika*

Cite This: *ACS Appl. Nano Mater.* 2023, 6, 1770−1782 Read Online

ACCESS | Metrics & More | Article Recommendations | Supporting Information

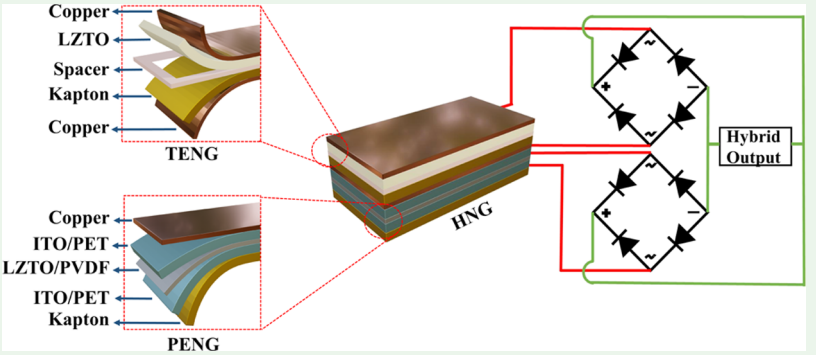

ABSTRACT: The need for technological innovation in competitive sports is crucial for self-monitoring and smart decision making. In this work, we demonstrate how intelligent sports and smart decision making can be achieved in cricket and boxing using lithium-modified zinc titanium oxide (LZTO) nanofibers based on piezoelectric nanogenerators (PENGs) and triboelectric nanogenerators (TENGs). Zinc titanium oxide (ZTO) nanofibers synthesized using electrospinning followed by a calcination technique are modified with lithium to increase the output of the nanogenerator. An optimized PENG is fabricated using 25 wt % loading of LZTO (d_{33} = 214 pm/V) in a poly(vinylidene fluoride) (PVDF) matrix as a double-layered structure and yields an open-circuit voltage (V_{oc}) of 35 V and a short-circuit current (I_{sc}) of 1.6 μA by manual tapping. To fabricate the TENG, Kapton and LZTO are used as negative and positive tribolayers, while Cu and adhesive polymer tape are used as the electrode and spacer, respectively. Furthermore, a hybrid nanogenerator (HNG) is fabricated by combining the PENG and TENG to produce a rectified voltage, current, and power density of up to 75 V, 3.2 μA, and 240 μW/cm^2, respectively. These HNGs are integrated with a punching bag and demonstrated to differentiate among the six types of punches in boxing. Furthermore, PENGs are used in cricket to monitor the number of balls middled on the bat during practice and the contact of the ball with the bat and stumps for smart decision making. All kinds of lab-scale testing are done for these applications, which pave a way for exploring the frontiers in nanogenerator applications in sports as maintenance-free and self-powered sensing technology.

KEYWORDS: *lithium-modified zinc titanium oxide, triboelectric nanogenerator, piezoelectric nanogenerator, hybrid nanogenerator, intelligent sports, decision making*

1. INTRODUCTION

The use of smart devices and sensors for the Internet of Things (IoT), cloud computing, and data collection in decision making has achieved massive consideration as a potential solution in the field of sports. In near future, the demand for smart devices by virtue of the dynamic advancement in the field of sports for information assortment and analysis may emerge as a significant issue for the player and the umpire to make decisions.[1] Despite the fact that many sensors have already been developed with high sensitivity and accuracy based on advanced technologies such as optical, capacitive, resistive, geomagnetic, chemical, and thermosensitive, the power utilization and intricacy in data acquisition remain a major issue.[1−4] In light of specific constraints including short life span, continuous substitution, and environmental toxicity, sensors based on nanogenerators have emerged as an ideal option due to their maintenance-free and self-powered sensing nature.[1] Generally, nanogenerators are used to generate electrical energy from different energy sources such as magnetic, thermal, and mechanical. Among different kinds of nanogenerators such as the pyroelectric nanogenerator, thermoelectric nanogenerator, triboelectric nanogenerator (TENG), and piezoelectric nanogenerator (PENG), nowadays,

Received: October 29, 2022
Accepted: January 19, 2023
Published: February 2, 2023

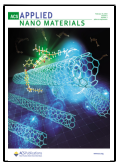

https://doi.org/10.1021/acsanm.2c04731
ACS Appl. Nano Mater. 2023, 6, 1770−1782

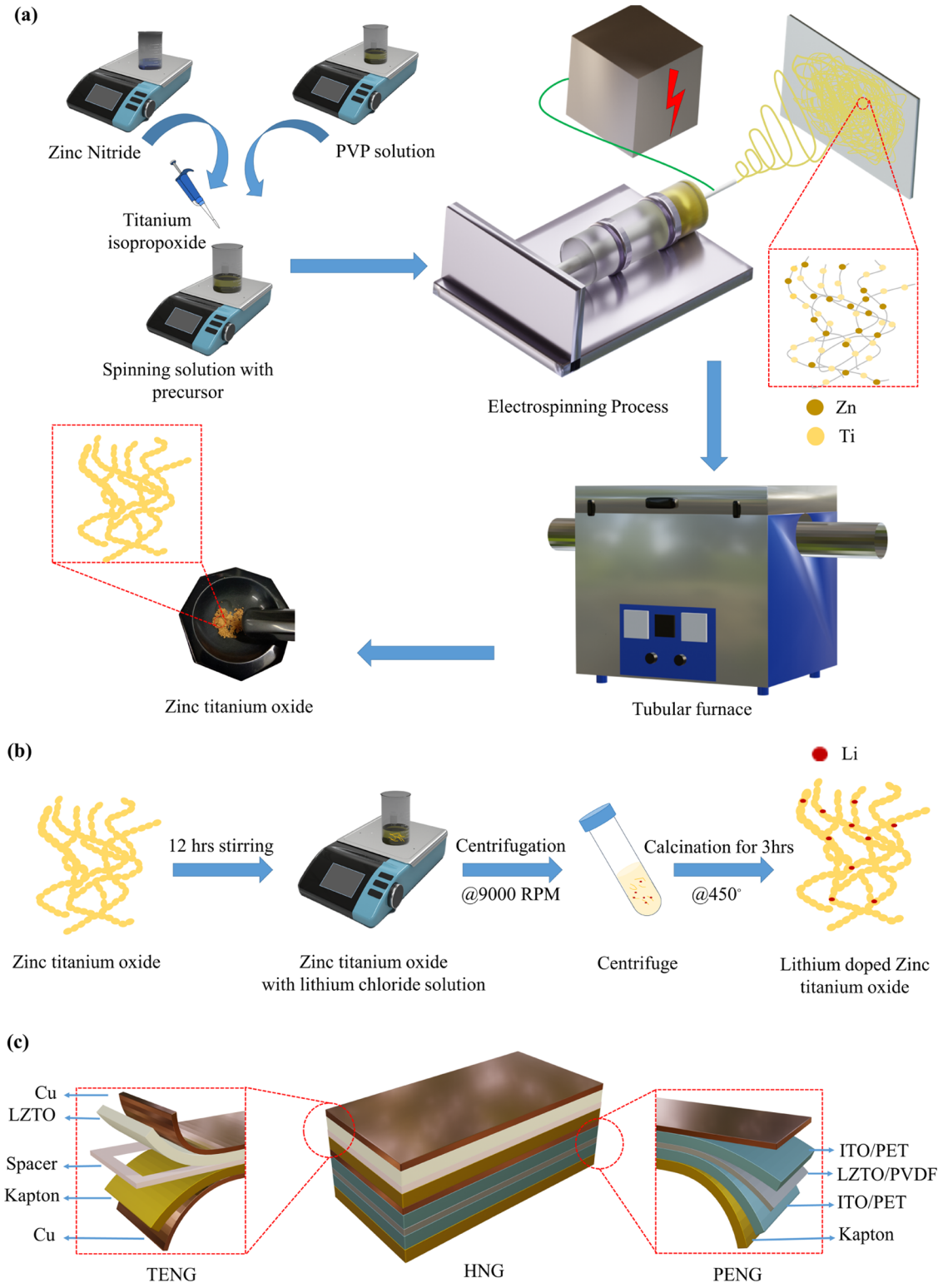

Figure 1. (a) Synthesis of zinc titanium oxide nanofibers (ZTO) by electrospinning followed by the calcination technique; (b) modification of ZTO nanofibers with lithium; and (c) schematic diagram of the TENG, PENG, and hybrid nanogenerator (HNG).

the TENG and PENG both have been commonly used as self-powered sensors and energy harvesters due to their distinct advantages.[1,5]

The TENG, which converts mechanical energy to electrical signals through the combination of two mechanisms, i.e., triboelectrification and electrostatic induction,[6] has emerged as a self-powered sensor because of its high voltage output, freedom of material selection, and size. Recently, TENG devices are reported as self-powered sensors, i.e., tactile, pressure, acceleration, and motion sensors.[7] Apart from TENGs, PENG are also a promising option for wearable, biomechanical, and sport-related sensors because of their flexibility, sensitivity, durability, and stability properties.[8] The PENG generates electricity by breakage of the crystal structure

https://doi.org/10.1021/acsanm.2c04731
ACS Appl. Nano Mater. 2023, 6, 1770−1782

from the central symmetry of the piezoelectric material caused by external mechanical stimuli.[9] Moreover, the PENG and TENG both are based upon the same type of mechanical vibration. Therefore, the synergistic combination of both the TENG and PENG can increase the potential of the nanogenerator without any substantial changes in its structure. The hybridized structure of the TENG and PENG can easily overcome the main disadvantage of the TENG, i.e., the high humidity dependency due to the temporary triboelectric charge. Therefore, substantial studies in the field of hybridized structures are growing, but the practical applications and cost viability still remain an issue of concern.

In this regard, novel materials that possess both piezo- and triboelectric properties are gaining significant interest.[10] The morphology, structure, and properties of the materials are the crucial factors for both piezo- and triboelectric effects to enhance the performance and sensitivity of the nanogenerator.[11] Piezoelectric materials in the form of polymers, ceramics, and their composites have already been used as TENGs to enhance the output. In polymer composites, the ceramic fillers act as a nucleating agent that helps obtain high piezoelectric coefficients. Furthermore, the high aspect ratio (AR) of the filler in the polymer matrix also helps increase the piezoelectric properties of the composite due to the easier formation of an interconnection pathway and low surface charges, which help reduce agglomeration.[12] To enhance the performance further, doping of the material with elements such as lithium, cobalt, and sodium showed great potential.[13] If the atomic radius of the dopant is higher or lower than that of the element, it creates lattice strain. Recent reports demonstrate the improvement in the piezoelectric performance via chemical doping of halogen elements that modulates the lattice strain along the ZnO polar *c*-axis.

Therefore, in this work, we have fabricated a novel piezo/triboelectric hybrid nanogenerator (HNG) in which the poly(vinylidene fluoride) (PVDF)/lithium-modified zinc titanium oxide (LZTO) nanofiber composite film acts as a piezoelectric film, with the LZTO nanofiber as a positive triboelectric material and Kapton tape as a negative triboelectric material. As PVDF has a low piezoelectric strain constant (d_{33}), we have used LZTO nanofibers as a filler to increase the output of the PVDF-based piezoelectric nanogenerator. In comparison to the previously reported PVDF-ZTO piezoelectric nanogenerators, we have achieved a higher output by lithium addition.[14] Here, the optimization of the LZTO concentration and structure was done to fabricate the PENG over an indium tin oxide (ITO)-coated poly(ethylene terephthalate) (PET) sheet, which acts as a current collector. Furthermore, the PENG was attached to a cricket bat to monitor the player's activity and to take the right decision during the match as a complimentary technique with ultraedge technology. It was also used on the stumps to indicate whether a ball has hit the stump or not. For the TENG, LZTO on conductive Cu was used as an electropositive material and Kapton tape on Cu was used as an electronegative tribomaterial. To further improve, the HNG was fabricated and used as a self-powered sensor in the field of intelligent sports as a wall-mounted boxing punching bag to monitor the activity of the player. This is the first report on a tribo/piezoelectric nanogenerator based on LZTO nanofibers for intelligent sports and smart decision making in lab-scale testing for cricket and boxing that the authors are aware of.

2. MATERIALS AND METHODS

2.1. Materials. Titanium(IV) isopropoxide ($Ti\{OCH(CH_3)_2\}_4$, 97%), zinc(III) nitrate hexahydrate ($Zn(NO_3)_2{\cdot}6H_2O$, 98%), lithium chloride (LiCl, ≥99.98), *N*,*N*-dimethylformamide (DMF, 99.8%), ethanol, poly(vinylpyrrolidone) (PVP) (average M_w ∼ 55,000), poly(vinylidene fluoride) powder (average M_w ∼ 180,000), conductive paste (silver) (≤35 μΩ cm), and indium tin oxide-coated poly(ethylene terephthalate) (ITO-PET) (≤10 Ω/sq) were bought from Sigma-Aldrich, India. Deionized (DI) water was used in this research work and was collected from the Millipore water purification setup (Merck, Direct Q 3-UV). Copper (Cu) tape (25 μm) was purchased from a local market in Hyderabad.

2.2. Methods. *2.2.1. Synthesis of Zinc Titanium Oxide Nanofibers.* Zinc titanium oxide nanofibers (ZTO) were synthesized following four steps as shown in Figure 1a

(i) Preparation of the precursor for ZTO and PVP spinning solution.
(ii) Electrospinning of poly(vinylpyrrolidone) (PVP) nanofibers with the precursor.
(iii) A two-step calcination process to obtain stable ZTO nanofibers.
(iv) Mild grinding of the ZTO nanofibers.

To maintain 1:1 molar ratio of the precursor, 1.487 g of $Zn(NO_3)_2$ was dissolved with 3 mL of DMF using a magnetic stirrer for 1 h, and then, 1.421 g of $Ti\{OCH(CH_3)_2\}_4$ was dropwise added to $Zn(NO_3)_2$ solution while stirring at 800 rpm. On the other side, the spinning solution was prepared by adding 6 g of PVP to 3 mL of DMF under continuous stirring. After preparation of the complete soluble precursor solution, the spinning solution was added to it and stirred for 4 h. In the next step, the properly mixed solution was loaded into a 5 mL plastic syringe and fiberized by electrospinning under 23 kV for 10 h, and the ZTO nanofibers were collected over an aluminum foil at a distance of 12 cm from the tip of the syringe. Then, the obtained PVP nanofibers with precursors were dried and calcined following a two-step calcination process according to the previously published work.[15] The nanofibers were stabilized first by heating up to 200 °C for 40 min with a holding time of 2 h, and in the second step, the temperature was ramped to 800 °C in 5 h and held for 2 h. Finally, the calcined mat was taken in a mortar and ground mildly using a pestle for 3 min.

2.2.2. Synthesis of Li^+-Modified ZTO Nanofibers. To prepare Li^+-modified nanofibers (LZTO), 1 g of ZTO nanofibers was dispersed in 100 mL of ethanol; later, 5 mL of 1 M LiCl/ethanol solution was added to it as a lithium source followed by continuous stirring for 12 h at room temperature. Then, the nanofibers were washed via centrifugation at 9000 rpm and dried. Finally, the dried product was calcined for 3 h at 450 °C to obtain the stable structure of LZTO. The graphical representation of the synthesis procedure is given in Figure 1b.

2.2.3. Fabrication of the Piezoelectric Nanogenerator. Double-layer and single-layer PENGs were fabricated by following a previously reported paper.[16] Different volume percentages, i.e., 10, 20, 25, and 30 vol %, of LZTO nanofibers were completely dispersed in DMF by ultrasonication for 2 h. Then, the fully dispersed solution was stirred continuously for 12 h with gradual addition of PVDF powder until a homogeneous LZTO/PVDF suspension was obtained. Furthermore, to fabricate single-layer LZTO/PVDF, the LZTO/PVDF suspension was spin-coated at 1000 rpm for 20 s on the ITO-coated PET followed by drying at 70 °C for 10 h. For double-layered LZTO/PVDF, as the name suggests, two steps were followed. In the first step, the LZTO/PVDF suspension was spin-coated at 1800 rpm for 12 s on an ITO-coated PET sheet and dried. In the second step, several drops of PVDF solution were again spin-coated on the LZTO/PVDF layer for the same 12 s at 1800 rpm and then dried on a hotplate for 2 h at 140 °C as shown in Figure S1, Supporting Information (SI). Finally, to fabricate the PENG, both single (SL)- and double-layered (DL) films were individually attached to another ITO-coated PET sheet over it to make a sandwich-like structure. Along with this, copper wires were connected to the surface of the

https://doi.org/10.1021/acsanm.2c04731
ACS Appl. Nano Mater. 2023, 6, 1770−1782

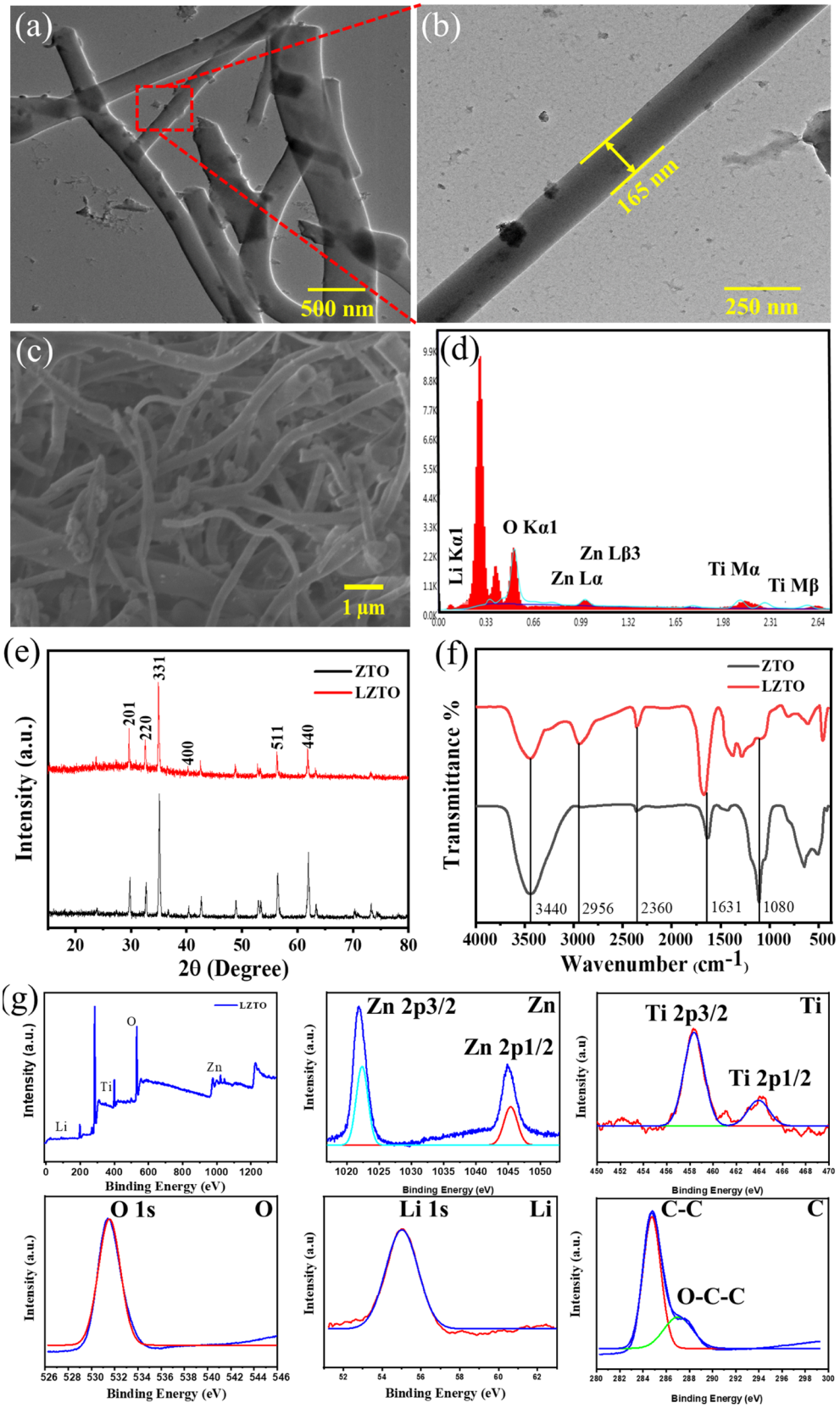

Figure 2. (a) TEM image; (b) magnified image of TEM; (c) SEM image; (d) EDS mapping of LZTO nanofibers; (e) compared XRD patterns, (f) FTIR spectra of both ZTO and LZTO; and (g) XPS data of LZTO nanofibers.

ITO-coated PET sheet with the aid of conducting silver paste for electrical conductive contact. Furthermore, the entire setup was wrapped with polyimide adhesive tape (Kapton) to make a stable compact structure. The as-fabricated single-layered (SL) LZTO/PVDF nanocomposite film- and double-layered (DL) LZTO/PVDF nanocomposite film-based devices with 10, 20, 25, and 30 vol %

https://doi.org/10.1021/acsanm.2c04731
ACS Appl. Nano Mater. 2023, 6, 1770−1782

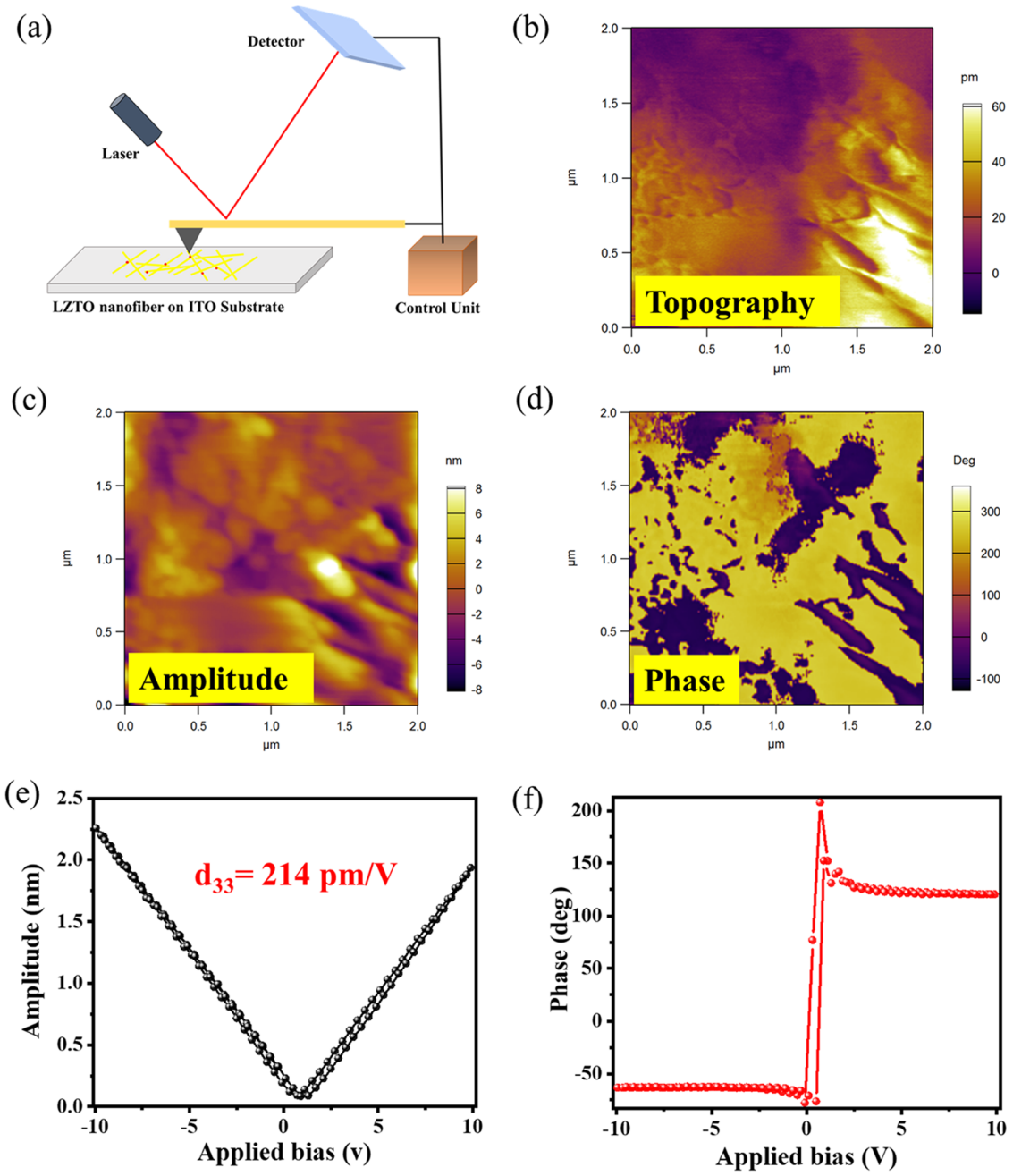

Figure 3. (a) Schematic of the PFM experimental setup; (b) PFM topography; (c) amplitude mapping; (d) phase mapping; (e) PFM displacement voltage curve; and (f) phase−voltage hysteresis loops of LZTO nanofibers.

LZTO were named as SL-P10, SL-P20, SL-P25, SL-P30 DL-P10, DL-P20, DL-P25, and DL-P30, respectively.

2.2.4. Fabrication of the Hybrid Nanogenerator. The LZTO-based HNG device fabrication process is schematically depicted in Figure 1c. In summary, the HNG was fabricated by combination of the TENG and PENG. For the TENG, LZTO nanofibers and Kapton tape were used as electropositive and electronegative tribomaterial, respectively, whereas for the PENG, the LZTO-PVDF composite film was used. Along with this, to achieve a compact structure of the HNG, one minor change was done in the design of the previously fabricated PENG. Here, the nonconductive side (upper) of the ITO/PET electrode was modified with a copper coating via the thermal evaporation technique, and then, the PENG was wrapped with Kapton tape to make a stable structure, which also acted as an electronegative tribomaterial. In addition to this, LZTO nanofibers were evenly applied over the adhesive side of Cu tape to fabricate the electropositive tribomaterial, where the extra material was removed by blowing air. The electropositive tribomaterial was then attached to the fabricated PENG by adding a spacer layer using an insulating polymer tape with double-side adhesion at the edges, leaving a square-shaped space at the center, in which the spacer supports the tribolayer to contact and separate easily. Finally, Cu leads were connected to the electrodes as conductive medium.

2.2.5. Instrumentation and Characterization. For the synthesis of LZTO nanofibers, electrospinning (E-Spin, Nanotech, India) and a tubular furnace (Sigma group of company, Chennai, India) were used. The composite LZTO-PVDF films were spin-coated using a spin coater (spinNXG-P1AC, Apex Instruments Co. Pvt. Ltd., India). For morphology characterization, a scanning electron microscope (ApreoLoVac with an additional energy-dispersive spectrometry (EDS) detector) and transmission electron microscope (JEM 2100, JEOL Ltd.) were used. In addition to this, the structural analysis of

https://doi.org/10.1021/acsanm.2c04731
ACS Appl. Nano Mater. 2023, 6, 1770−1782

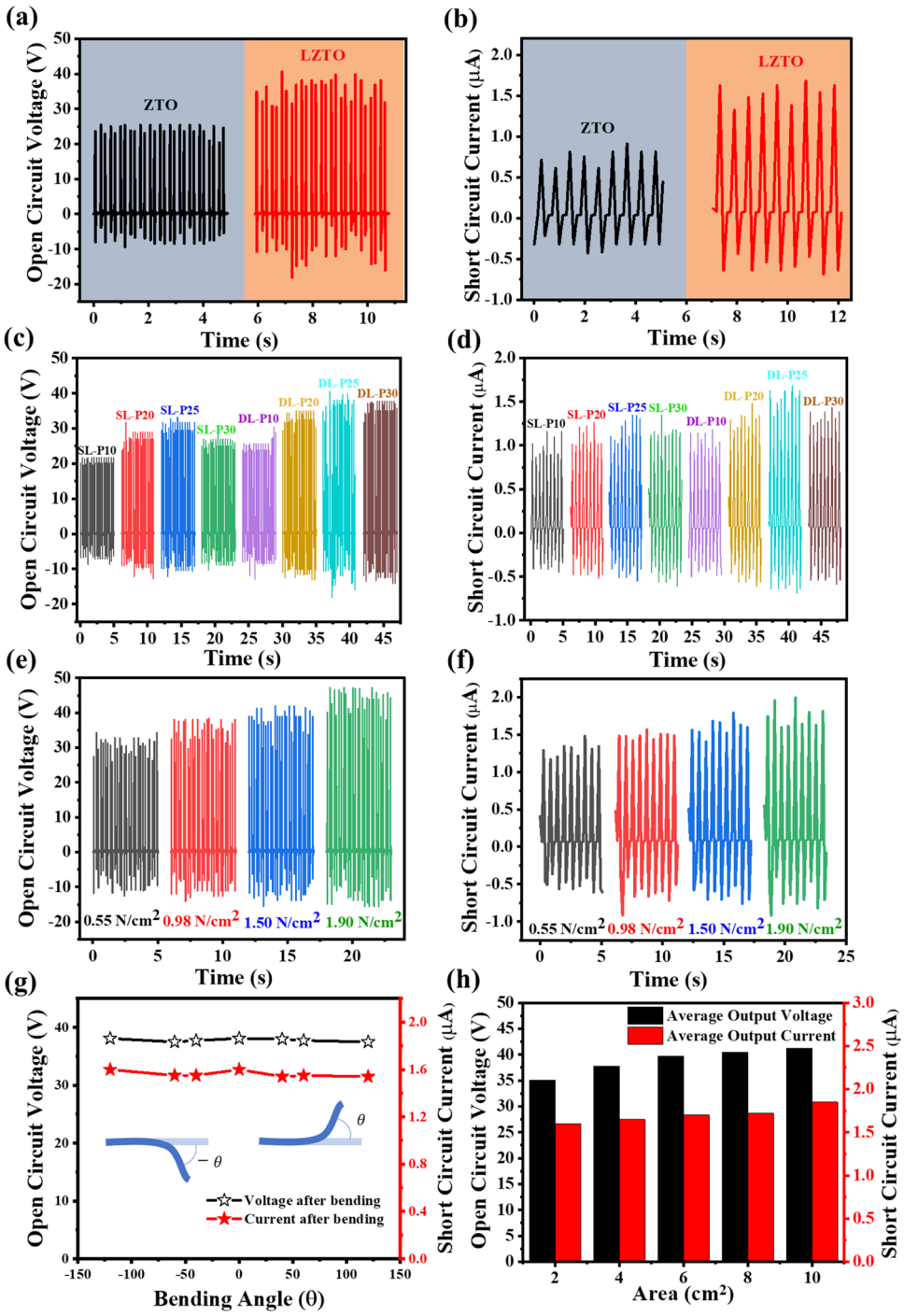

Figure 4. (a) Open-circuit voltage (V_{oc}) and (b) short-circuit current (I_{sc}) of the piezoelectric nanogenerator with and without Li; (c) open-circuit voltage (V_{oc}) and (d) short-circuit current (I_{sc}) with different LZTO nanofiber concentrations; (e) open-circuit voltage (V_{oc}) and (f) short-circuit current (I_{sc}) of DL-P25 under different forces; (g) average voltage and current output after and before bending; and (h) average voltage and current output of DL-P25 with different dimensions of active area.

the material was done using an X-ray diffractometer (XRD, Bruker Discover D8 with Cu Kα radiation). Furthermore, a Thermo Scientific Nicolet iS5 Fourier transform infrared (FTIR) spectrometer was used to study the presence of functional groups, and X-ray photoelectron spectroscopy (XPS, Axis Supra, Kratos analytical) was used to determine the chemical bonding. All the electrical characterization (output voltage and output current) was performed using a digital storage oscilloscope (Agilent Technologies, DSO 3062A) and a sourcemeter (Keithley, Tektronix, 2450).

3. RESULTS AND DISCUSSION

3.1. Morphological and Structural Characterization.

The morphological analysis of LZTO nanofibers performed via transmission electron microscopy (TEM) shown in Figure 2a,b reveals the formation of pure LZTO nanofibers. The higher resolution magnified image of a single LZTO nanofiber shown in Figure 2b gives an idea about the average diameter of LZTO nanofibers, which is around 165 nm. In addition to this, agglomerations of the material were found to be formed as

https://doi.org/10.1021/acsanm.2c04731
ACS Appl. Nano Mater. 2023, 6, 1770−1782

beads that are given in Figure S2. The scanning electron microscopy (SEM) image shown in Figure 2c indicates the nanofiber structure of LZTO, corroborating well with TEM. In Figure S3, the LZTO nanofiber shows a slight reduction in the diameter in comparison to the PVP nanofiber with the precursor, which might be due to the removal of PVP during calcination. However, the morphology of ZTO still remains smooth after calcination due to a slow heating rate, which avoids the rapid evaporations of PVP and solvents. EDS mapping also confirmed the existence of Li, Zn, Ti, and O in LZTO nanofibers as shown in Figure 2d.

The structural analysis of ZTO nanofibers and LZTO nanofibers was performed via X-ray diffraction (XRD), as depicted in Figure 2e. The XRD pattern of ZTO showed the structure as $ZnTiO_3$ having a hexagonal structure corresponding to the JCPDS File Card No. 26-1500.[17] In addition to this, a pseudocubic symmetry of ZTO can also be observed that is mildly distorted from the ideal cubic structure due to the existence of some impurities.[14] There is no extra lithium peak shown other than ZTO in the graph because of the identical ionic radii of Zn^{2+} and Li^{+}.[13,18,19] Possibly, the Zn atom is only replaced by lithium because calcination was performed for the second time at 450 °C.

FTIR spectra of ZTO and LZTO shown in Figure 2f exhibit peaks at ∼3440 and ∼1631 cm^{-1} that correspond to the O−H stretching and H−O−H bending mode vibrations, respectively, indicating more moisture content at the surface of the material. The peaks at ∼2360 cm^{-1} can be attributed to the adsorbed carbon dioxide from the atmosphere. Furthermore, peaks at ∼1080 cm^{-1} correspond to the symmetric C−O bond, which is reduced in the LZTO sample because of the calcination performed for the second time.[20] Then, peaks at ∼510 and ∼640 cm^{-1} were ascribed to the Ti−O stretching vibration, whereas the characteristic peak at ∼430 cm^{-1} was attributed to the Zn−O stretching vibration. Additionally, the peaks at ∼790 cm^{-1} correspond to the substitution of Zn atoms with Li. Furthermore, the peaks observed between 800 and 400 cm^{-1} in LZTO are different from those of ZTO, which can be considered to be due to the Li modification.

X-ray photoelectron spectroscopy (XPS) was performed to obtain the elemental bonding states of LZTO as depicted in Figure 2g. Here, the Zn 2p has split into two peaks (Zn $2p_{3/2}$ and Zn $2p_{1/2}$) as shown at 1022.43 and 1045.43 eV, indicating the formation of Zn−O.[21] Then, the Ti 2p spectrum with two distinguished peaks at 468.23 and 484.13 eV was attributed to $2p_{3/2}$ and Ti $2p_{1/2}$, respectively. Furthermore, the O 1s peak at 529.86 eV shows the formation of oxide in the material and the peak at 55.26 eV corresponds to the characteristic signals of Li 1s. The C peak presence at 284.8 eV indicates the carbon present in the carbon tape, which is used for characterization.

3.2. Piezoresponse Force Microscopy (PFM). The LZTO sample coated over the conductive ITO surface was used under a silicon tip for the piezoresponse force microscopy (PFM) characterization as depicted in Figure 3a. The topography, amplitude, and phase image were captured over the 2 μm × 2 μm scan area as given in Figure 3b−d, respectively. The PFM phase image obtained under the applied voltage depicts the local polarization orientation. The asymmetric butterfly loop-based amplitude signal graph exhibited in Figure 3e indicates barrier potential difference between the electrode and sample and the existence of the internal built-in electric field of the LZTO as well.[22] Furthermore, the piezoelectric nature of the LZTO nanofibers was confirmed from the hysteresis loop depicted in Figure 3f, which is due to the presence of two discrete polarization states with 120° phase difference.[23] Finally, the d_{33} value of the LZTO nanofibers was calculated as 214 pm/V from the slope of the butterfly loop. The shift of the loop that occurred toward the positive side shows the existence of the internal electric field that is caused by the mechanical stress exerted by the silicon tip and electrostatic effect induced due to the surface potential.[24,25]

3.3. Characterization of the PENG. The effect of lithium on the output of open-circuit voltage (V_{oc}) and short circuit current (I_{sc}) of the LZTO nanofiber−PVDF composite was studied by manually applying compressive force in a vertical direction. The variation in the output of V_{oc} and I_{sc} peaks was observed because of the manual hand tapping. The PENG with lithium and only the ZTO nanofiber-based composite depicted in Figure 4a,b confirms the increase in both V_{oc} and I_{sc} values in the presence of lithium. As atomic substitution of Zn in ZTO with Li atoms creates a large difference in atomic radius (calculated atomic radius) between Zn (142 pm), Ti (176 pm), O (48 pm), and Li (167 pm), the output of LZTO was observed to be higher.[13,26] The average value of V_{oc} (peak to peak) of ZTO and LZTO is 25 and 35 V, respectively. Similarly, the average value of I_{sc} (peak to peak) is 0.75 and 1.6 μA in the same order. From this, it is clearly observed that the V_{oc} and I_{sc} of LZTO are almost 1.5 times and 2 times, respectively, higher than those of the unmodified ZTO. Furthermore, the experiment was performed in the form of single-layer and double-layer LZTO-PVDF composite films with different concentrations of LZTO nanofibers, and the observed outputs of those PENGs are exhibited in Figure 4c,d. With increasing percentage of LZTO nanofibers in the composite, the average values of V_{oc} and I_{sc} are also increased. The average peak values of V_{oc} for SL-P10, SL-P20, SL-P25, and SL-P30 are 22, 28, 30, and 25 V, respectively, and the average peak values of I_{sc} are 0.8, 1.1, 1.3, and 1.15 μA in the same order. The increasing tendency of the output of the PENG with increasing percentage up to 25% of the electroactive material (LZTO) is easy to understand because of the high amount of polarization generation in the nanofiber−matrix interface, but a further increase in the concentration resulted in a decrease in the output because the threshold concentration of LZTO is 25%. The outputs of the double-layer (DL) film are much higher than those of the single-layer (SL) film with the same loading of nanofibers in the composite. For example, the average V_{oc} of the double-layer composite-based piezoelectric nanogenerator with 25% loading of LZTO (DL-P25) is 35 V, which is much higher than that of the single-layer composite-based PENG with 25% loading of LZTO (SL-P25). The output enhancement can be explained based on two reasons; first, the defect which occurs on the surface of the composite during the process of synthesis is filled by the neat PVDF second layer, which helps for the smooth transformation of the applied force to the LZTO nanofibers through the matrix. Second, the inductive charge is stored in between the additional heterogeneous interface layer of LZTO/PVDF and PVDF that helps increase the output. Here, the heterogeneous double-layered piezoelectric nanogenerator also benefits the uniform distribution of the force throughout the film.[16] The force-dependent output V_{oc} and I_{sc} of LZTO/PVDF-based PENG were recorded under different forces, which are given in Figure 4e,f, respectively. The V_{oc} average peak values at 0.55, 0.98, 1.50, and 1.90 N/cm^2 are 32,

https://doi.org/10.1021/acsanm.2c04731
ACS Appl. Nano Mater. 2023, 6, 1770−1782

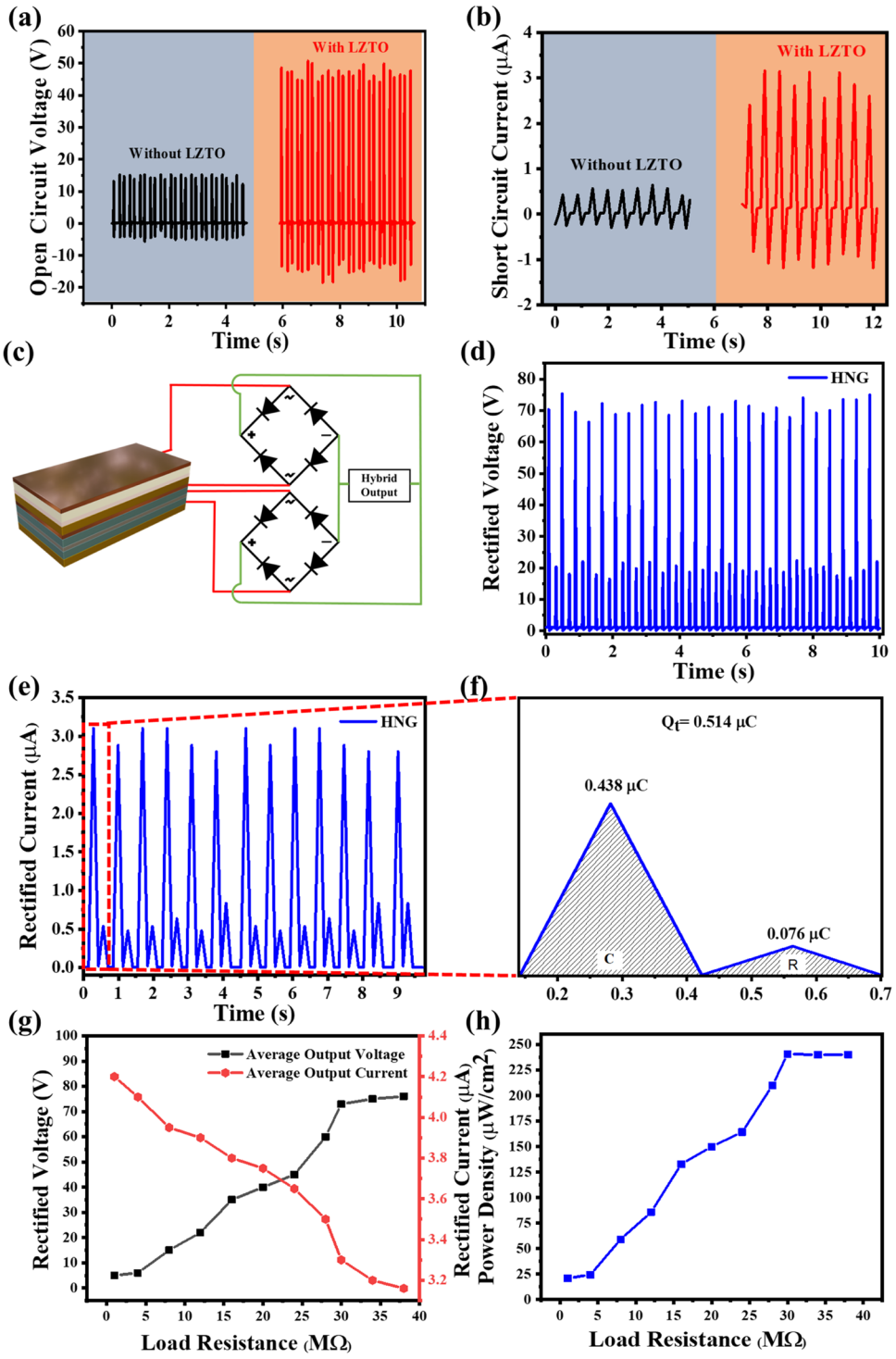

Figure 5. (a) Open-circuit voltage (V_{oc}) and (b) short-circuit current (I_{sc}) of the TENG with and without LZTO; (c) schematic of the HNG circuit diagram for rectification; (d) rectified voltage of HNG; (e) rectified current of the HNG; (f) charge stored by the HNG per cycle; (g) average value of rectified voltage and rectified current with different external load resistances; and (h) power density with different external load resistances.

36, 40, and 45 V, respectively. The I_{sc} average peak values are 1.2, 1.4, 1.6, and 1.65 μA in the same order as mentioned previously. The gain in output with the force increase was achieved because of the increasing trend of the dipole polarization at the polymeric interlayer. The arrangement and calculation to measure the force given by finger tapping are shown in Section S1. The sensitivity (S) of the LZTO/PVDF-based PENG was calculated according to the formula $S = \frac{\Delta V}{\Delta F}$ and $\frac{\Delta I}{\Delta F}$, where ΔF, ΔV, and ΔI are the increase of force, voltage, and current, respectively. When the applied force reached 1.9 N from 0.55 N, the voltage and current sensitivity was observed to be 10.37 V/N and 370.37 nA/N, respectively. To study the flexibility of the nanogenerator, the V_{oc} and I_{sc} of the LZTO/PVDF-based PENG were recorded before and after bending at different bend angles for 50 cycles.

https://doi.org/10.1021/acsanm.2c04731
ACS Appl. Nano Mater. 2023, 6, 1770−1782

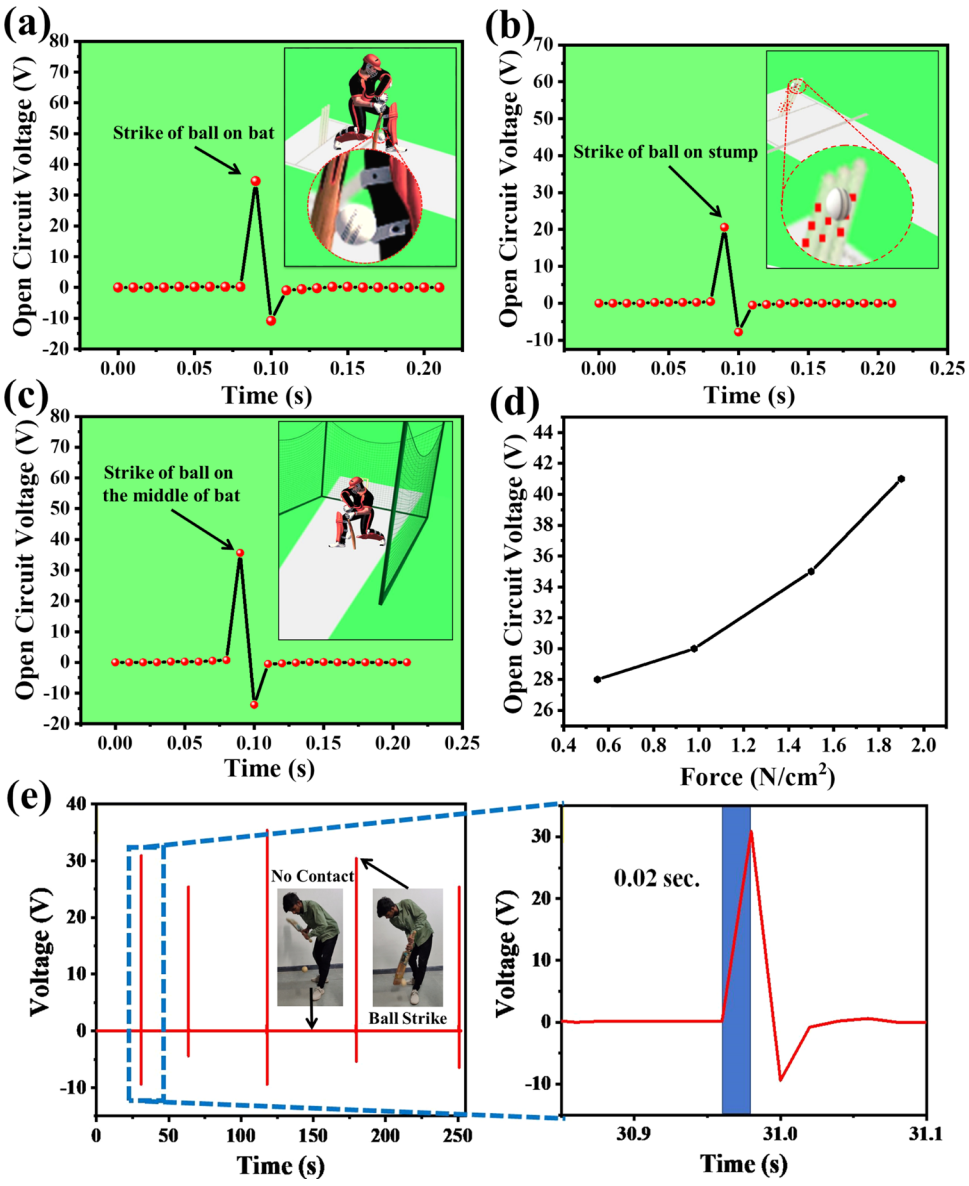

Figure 6. PENG used for decision making. (a) Strike of the ball on the bat; (b) strike of the ball on the stump; (c) middling of the ball on the bat during net practice; (d) voltage output under various forces on the bat; and (e) voltage output of each strike of the ball on the bat with an enlarged graph indicating the response time of a single strike.

The average V_{oc} and I_{sc} are exhibited in Figure 4g at 120, 60, and 30° in both up and down directions, which reveal the good stability nature of the nanogenerator, as the changes in V_{oc} and I_{sc} are negligible. In Figure 4h, the average V_{oc} and I_{sc} of PENGs at the different active areas were observed at a particular force. The V_{oc} values of the PENG at 2, 4, 6, 8, and 10 mm^2 are 35, 37, 40, 41, and 42 V, respectively. The I_{sc} values of the PENG are 1.6, 1.7, 1.8, 1.85, and 1.9 μA in the same order as mentioned previously. Despite a huge increase in the area, the output did not increase much because of the same applied force over the area for all the PENGs. The polarity check test was also performed for both voltage and current by interchanging the connection of the output load, which is exhibited in Figure S5a,b.

The PENG generates electromotive force from mechanical stimuli because of the noncentrosymmetric crystal structure of both LZTO and PVDF. With no external force, dipoles inside the LZTO/PVDF composite are in a random orientation, but due to mechanical stimuli, the dipoles are arranged in one direction and generate voltage across the material. Because of compression and relaxation, the LZTO/PVDF composite piezoelectric materials generate positive and negative polarity voltage, respectively. This improvement in the piezoelectric reaction of the LZTO-PVDF composite is a direct result of the electroactive phase of PVDF, higher unconstrained polarization of LZTO, and high AR of LZTO.[12,27] The schematic portrayal representing the working mechanism of the PENG is exhibited in Figure S6.

3.4. Characterization of the TENG. The TENG was fabricated using Kapton tape as an electronegative tribolayer and LZTO as an electropositive tribolayer. Here, Cu and an adhesive polymer layer was used as an electrode and spacer, respectively. In this study, the TENG (1.4 cm × 1.4 cm) based on LZTO was fabricated with a 0.2 cm-width spacer at each side. Therefore, the main working area reduced to 1 cm × 1 cm.

https://doi.org/10.1021/acsanm.2c04731
ACS Appl. Nano Mater. 2023, 6, 1770−1782

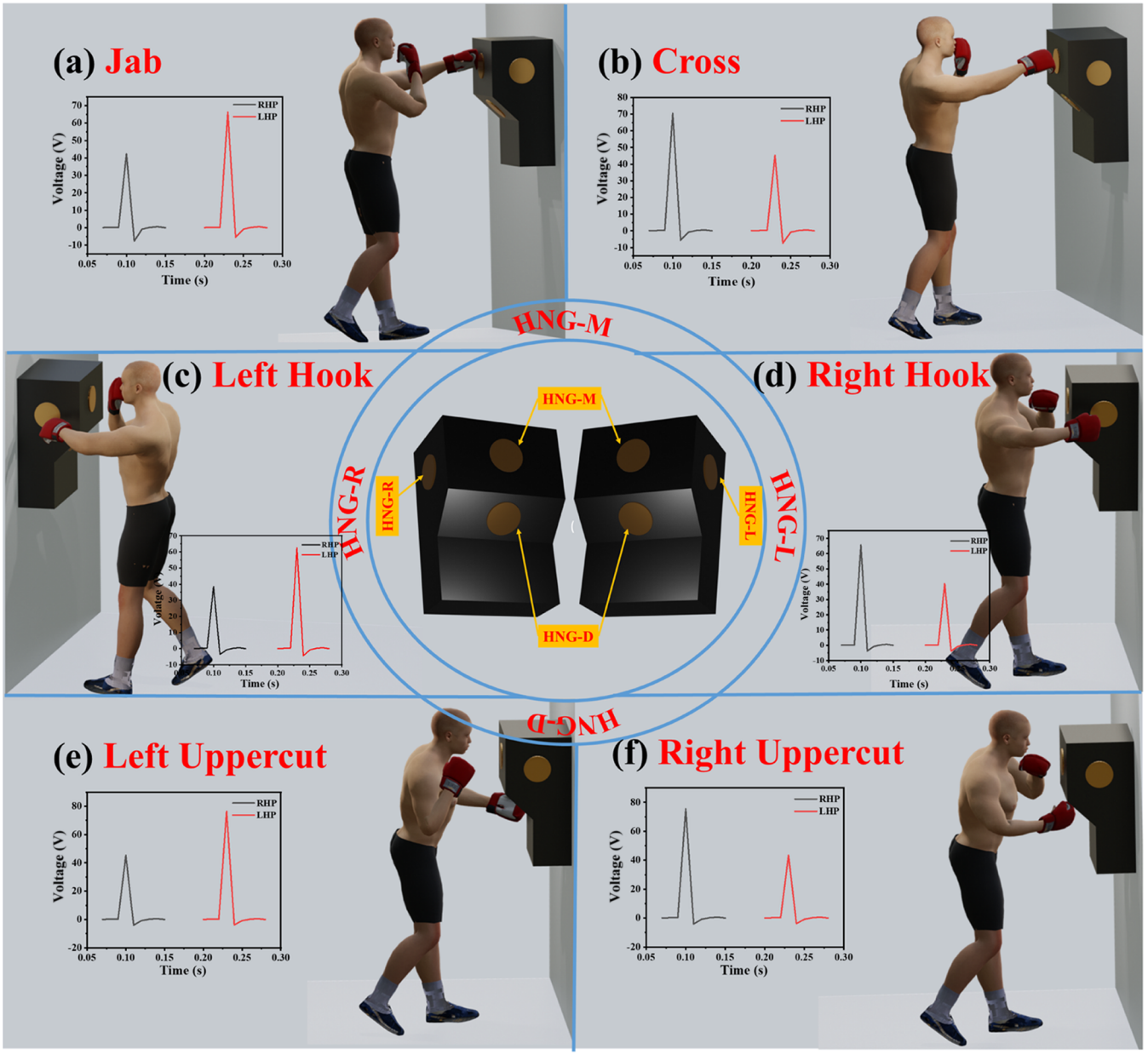

Figure 7. Schematic and voltage output of different punches by both a RHP and LHP, (a) jab; (b) right cross; (c) left hook; (d) right hook; (e) left uppercut; and (f) right uppercut.

The detailed output of V_{oc} and I_{sc} of the TENG (1 cm × 1 cm) is depicted in Figure 5a,b respectively. The V_{oc} and I_{sc} output peaks reached up to 70 V and 3.05 μA, respectively, by hand tapping, and the test was performed many times to check the reproducibility and accuracy of the data. For comparison, Cu was used as the only electropositive material (without LZTO) with Kapton tape, which showed the V_{oc} and I_{sc} output peaks at 15 V and 0.5 μA, respectively.

Due to the external force, the LZTO layer and Kapton layer came into contact, because of which the atoms present at LZTO, especially oxygen, donated their electrons to the Kapton tape. As a result, the Kapton tape's surface became negatively charged and LZTO nanofibers became positively charged. Upon removal of the external force, the free electrons flow from the Kapton tape to LZTO through their respective electrodes. Hence, both electrodes became charged by the induced charge, and the external connection transported the current. The contact between LZTO and Kapton tape for the second time under the external load resulted in a reverse current flow in the external circuit due to the backflow of electrons. In this way, the cycles of voltage and current generation continued till the external force stopped. The structure of LZTO was found to be stable even after 1000 cycles of mechanical stimuli by comparing the before and after SEM image of LZTO as shown in Figure S7.

3.5. Characterization of the HNG. To get higher output, the PENG and TENG were combined to fabricate a hybrid nanogenerator (HNG) and the output of V_{oc} and I_{sc} was observed multiple times by hand tapping. The HNG was integrated with two full-bridge rectifiers, where the TENG was connected to one and the other one was connected with the PENG to get rectified output as depicted in the schematic diagram in Figure 5c. The rectified voltage and current outputs were 75 V and 3.2 μA, respectively, as given in Figure 5d,e. As

https://doi.org/10.1021/acsanm.2c04731
ACS Appl. Nano Mater. 2023, 6, 1770−1782

Table 1. Comparison of the Hybrid Nanogenerator with the Previously Reported Few Similar Studies

material	material structure	hybridization details	active area (cm^2)	voltage (V)	current (μA)	power density ($\mu W/cm^2$)	reference
ZnO	nanorod	ZnO/PVDF composite for the PENG and TENG with PTFE	1.8	78	0.46	24.5	30
PVDF	nano/microfiber	PDVF as PENG and PDMS as TENG with Cu	0.07	1.2	0.03		31
$BaTiO_3$	nanoparticle	cellulose/$BaTiO_3$ aerogel paper-based PDMS composite for the PENG and PDMS and skin as the TENG	4	48		21.25	32
P(VDF-TrFE)	nanofiber	P(VDF-TrFE) as piezoelectric and PDMS-MWCNT as triboelectric with Ag	0.64	17			33
$BaTiO_3$	particle	$BaTiO_3$-PDMS film	3	3.3			34
lithium-doped zinc titanium oxide	nanofiber	double-layer structure of LZTO and PVDF as the PENG and LZTO as the tribolayer	1	75	3.2	240	this work

the outputs of the two mechanisms (triboelectric and piezoelectric) are connected parallelly, the rectified voltage and current of the HNG were slightly higher than those of the individual one. Furthermore, the charge produced in each compression and relaxation cycle was calculated for the HNG by calculating the area under the rectified current curve. Because of this continuous cycle of compression and relaxation, two peaks combined to make up one cycle of the rectified current signal.[28] Therefore, the charge of one cycle of the HNG was observed by calculating conjugate 2 peaks, which was around 0.438 and 0.076 μC as depicted in Figure 5f. To calculate the instantaneous power of the HNG at different resistances, the average voltage and current were observed at different resistances from 100 Ω to 40 MΩ, as given in Figure 5g,h. With an increasing trend of resistance, the current decreased, while the voltage increased. As a result, the power density of the HNG increased up to 240 $\mu W/cm^2$, which was calculated by the multiplication of the average voltage and average current as the working area of the HNG (1 cm × 1 cm).

3.6. Applications. *3.6.1. Application of the PENG in Cricket for Smart Decision Making and Self-Monitoring.* The LZTO/PVDF composite-based PENG was developed as a low-cost, self-powered, maintenance-free sensor for the detection of the ball's contact with the bat and stumps, which will help referees to make the right decision. Furthermore, the PENG was used to monitor the middling of the ball on the bat, which can be useful during practice sessions for the players.

In this work, the PENG was attached on the bat and the output voltage of the PENG was recorded with every strike of the ball on the bat. Here, a unified output of V_{oc} peaks was observed because of the shock load by the ball. As shown in Figure 6a, each strike generates voltage, which indicates the contact of the ball on the bat. Despite the variation in signals (output voltage) of the PENG due to different factors such as the contact position, speed of the ball, and force applied by the batsman to hit the ball, the output signal will be considered a strike of the ball on the bat, which will help the referee of the match to make the correct decision. Likewise, the signal (voltage output) of the PENG due to the connection of the ball on stumps shown in Figure 6b also plays a crucial role in deciding whether the player is dismissed or not. The signal from the stump refers to information about the connection of the ball on the bat. For the self-monitoring during the practice session, the area of the PENG was reduced to 5 cm × 5 cm and attached to the middle of the bat at which the ball should hit for the perfect shot. The signal from the PENG corresponds to the ball strike on the bat in a perfect manner as depicted in Figure 6c. This sensor's signal varies with the variation of force with the change in speed of the ball as given in Figure 6d. Furthermore, the pressure sensitivity of the PENG as a sensor could reach up to 10.01 V/N as per the calculation by linear fitting, which showed the ability of the sensor to sense the applied force. On the other hand, increasing response time (i.e., time taken by the sensor to achieve from 10 to 90% of its final value) is a key factor during the real-time signal monitoring and helps determine the efficiency of this proposed approach in smart decision making as shown in Figure 6e.[29] The response time was found to be 0.02 s, which is significantly faster. The overall performance and the ultrafast response of the LZTO/PVDF-based PENG therefore establish it as a superior sensing technology for self-monitoring along with decision making in cricket over the traditional technologies used for the same.

3.6.2. Application of the HNG in Boxing to Differentiate between Types of Punches. A HNG-based wall-mounted punching bag was developed, by which different kinds of punches can be monitored, that can be used by boxers to self-monitor the type of punches they deliver. A total of four HNGs (5 cm × 5 cm) were attached over the different sides of the punching bag as shown in Figure 7. As per boxing rules, there are mainly six types of basic punches, which can be detected by our proposed model. Using this setup, jab and cross, which are similar punches but registered from the left hand and right hand, respectively, can be detected by the HNG, which is at the middle of the punching bag and mentioned as HNG-C. Similarly, the right cross and left cross named HNG-R and HNG-L can be detected on the right and left sides of the punching bag, respectively. Along with this, left uppercut and right uppercut can also be detected on HNG-D, when it is attached to the bottom portion of the punching bag.

In this work, the voltage outputs from the impact of the punch were observed for two different players, one being a right-handed player (RHP) and the other being a left-handed player (LHP) as shown in Figure 7a–f. For the ease of comparison and interpretation, both players were from the same age, gender, and weight categories. The voltage outputs of the RHP's jab and right cross were observed to be 42.4 and 70.5 V, respectively, which signifies that the RHP has more strength in the right hand than in the left hand. This is in agreement with the general pattern observed for left-handers and right-handers in boxing. Similarly, the voltage outputs of the LHP's jab and right cross were found to be 66.3 and 45.3 V, respectively. The voltage outputs of 38.7 and 62.6 V were generated by the left hook of the RHP and LHP, respectively, whereas the voltage output of 66 and 40.34 V were generated by the right hook of the RHP and LHP correspondingly.

https://doi.org/10.1021/acsanm.2c04731
ACS Appl. Nano Mater. 2023, 6, 1770−1782

Likewise, the voltage output of the left uppercut and right uppercut was 45.7 and 76.4 V for the RHP and 75.3 and 44 V for the LHP, respectively. As can be seen from the magnitudes of the output signals generated from different types of punches, there exists a wide variation in the signals (voltage output) generated by the HNGs. This leads to easy identification of each type of punch delivered by the boxer. For easy understanding, the combined data of the four HNG signals (voltage output) during the practice session of the RHP are shown in Figure S8a. The signals of HNGs can also be used to analyze the speed of the player (punch per second) by calculating the number of signals observed per second as shown in Figure S8b. As can be observed from all the data, the developed sensor based on the HNG could precisely detect all the basic punches of boxing of a player from the specific real-time information in the form of graphs and numerical values.

The comparison data of the fabricated LZTO-based piezo/triboelectric hybrid nanogenerator with few previously reported studies based on hybrid nanogenerators are shown in Table 1. The nanowire-structured Zn-O/PVDF composite-, PVDF micro/nanofiber-, cellulose/ $BaTiO_3$ paper-, PVDF-TrFE nanofiber-, and $BaTiO_3$ particle/PDMS composite-based PENGs combined with TENGs were reported previously; however, voltage and current outputs are significantly lesser.[30−34] The as-fabricated HNG is an excellent choice for self-powered sensors because of the higher current, voltage, and power density and excellent sensitivity, durability, and stability.

4. CONCLUSIONS

In summary, a lithium-modified ZTO nanofiber (LZTO)-based tribo/piezoelectric nanogenerator for intelligent sports and smart decision making was demonstrated. The TENGs and PENGs were combined to fabricate HNGs, which can be used as a self-powered sensor and a mechanical energy harvester. To fabricate the PENG, the synthesized LZTO nanofibers were reinforced into a PVDF matrix and a composite, obtained in the form of single-layered and double-layered PENGs, respectively, in which the DL-based PENG at the same concentration of LZTO produced a higher output compared to that of the SL-based PENG. To fabricate the HNG, Kapton tape and LZTO were used as negative and positive tribolayers, respectively, which produced a rectified voltage, current, and power density of 75 V, 3.2 μA, and 240 $\mu W/cm^2$, respectively. These HNGs were integrated with a punching bag and demonstrated to differentiate among the six types of punches in boxing. Along with this, PENGs were used in cricket to monitor the number of balls middled on the bat during practice and the contact of the ball with the bat and stumps for smart decision making. The work demonstrated here presents a way forward toward the use of nanogenerators in competitive sports.

ASSOCIATED CONTENT

Supporting Information

The Supporting Information is available free of charge at https://pubs.acs.org/doi/10.1021/acsanm.2c04731.

Schematic diagram of steps followed for double-layer piezoelectric nanogenerator fabrication; TEM image of LZTO nanofibers with accumulation of materials as beads; SEM image of PVP nanofibers with precursors and ZTO nanofibers; real image of the integrated device of 1 cm × 1 cm dimension as per scale; forward and reverse connections of PENG V_{oc} and I_{sc}; working mechanism of the PENG; SEM image of the LZTO film before and after 1000 cycles of mechanical pulse; voltage output of continuous punches and speed of the RHP during practice; and simple arrangement for the measurement done using a weighing scale (PDF)

Real-time demonstration of middling of the ball on the bat during practice (MP4)

AUTHOR INFORMATION

Corresponding Author

Sushmee Badhulika − *Department of Electrical Engineering, Indian Institute of Technology Hyderabad, Hyderabad 502285, India;* orcid.org/0000-0003-3237-3031; Email: sbadh@iith.ac.in

Authors

Nishat Kumar Das − *Department of Electrical Engineering, Indian Institute of Technology Hyderabad, Hyderabad 502285, India;* orcid.org/0000-0002-5553-964X

Om Priya Nanda − *Department of Electrical Engineering, Indian Institute of Technology Hyderabad, Hyderabad 502285, India;* orcid.org/0000-0002-8749-7982

Complete contact information is available at: https://pubs.acs.org/10.1021/acsanm.2c04731

Author Contributions

N.K.D.: conceptualization, methodology, data curation, writing—original draft preparation, and writing—reviewing and editing; O.P.N.: methodology, writing—original draft preparation, and writing—reviewing and editing; and S.B.: conceptualization, funding acquisition, investigation, project administration, resources, supervision, and writing−review and editing.

Notes

The authors declare no competing financial interest.

ACKNOWLEDGMENTS

This research work has received financial assistance from the Defense Research Development Organization funding (DRDO) grant DYSL-AST/CARS/CONTRACT/20-21/02.

REFERENCES

(1) Luo, J.; Gao, W.; Wang, Z. L. The triboelectric nanogenerator as an innovative technology toward intelligent sports. *Adv. Mater.* **2021**, *33*, No. 2004178.

(2) Leber, A.; Cholst, B.; Sandt, J.; Vogel, N.; Kolle, M. Stretchable optical fibers: Stretchable thermoplastic elastomer optical fibers for sensing of extreme deformations (Adv. Funct. Mater. 5/2019). *Adv. Funct. Mater.* **2019**, *29*, No. 1970030.

(3) Schwartz, G.; Tee, B. C.; Mei, J.; Appleton, A. L.; Kim, D. H.; Wang, H.; Bao. Flexible polymer transistors with high pressure sensitivity for application in electronic skin and health monitoring. *Nat. Commun.* **2013**, *4*, No. 1859.

(4) Yamada, T.; Hayamizu, Y.; Yamamoto, Y.; Yomogida, Y.; Izadi-Najafabadi, A.; Futaba, D. N.; Hata, K. A stretchable carbon nanotube strain sensor for human-motion detection. *Nat. Nanotechnol.* **2011**, *6*, 296−301.

(5) Veeralingam, S.; Badhulika, S. Ti@MoS2 incorporated Polypropylene/Nylon fabric-based porous, breathable triboelectric nanogenerator as respiration sensor and ammonia gas sensor applications. *Sensors and Actuators B: Chemical* **2023**, *380*, 133346.

(6) Wang, Z. L. Triboelectric nanogenerator (TENG)—sparking an energy and sensor revolution. *Adv. Energy Mater.* **2020**, *10*, No. 2000137.
(7) Wang, H.; Cheng, J.; Wang, Z.; Ji, L.; Wang, Z. L. Triboelectric nanogenerators for human-health care. *Sci. Bull.* **2021**, *66*, 490−511.
(8) Mao, Y.; Shen, M.; Liu, B.; Xing, L.; Chen, S.; Xue, X. Self-powered piezoelectric-biosensing textiles for the physiological monitoring and time-motion analysis of individual sports. *Sensors* **2019**, *19*, No. 3310.
(9) Mason, W. P. Piezoelectricity, its history and applications. *J. Acoust. Soc. Am.* **1981**, *70*, 1561−1566.
(10) Shaukat, R. A.; Saqib, Q. M.; Kim, J.; Song, H.; Khan, M. U.; Chougale, M. Y.; Bae, J.; Choi, M. J. Ultra-robust tribo-and piezo-electric nanogenerator based on metal organic frameworks (MOF-5) with high environmental stability. *Nano Energy* **2022**, *96*, No. 107128.
(11) Lei, H.; Chen, Y.; Gao, Z.; Wen, Z.; Sun, X. Advances in self-powered triboelectric pressure sensors. *J. Mater. Chem. A* **2021**, *9*, 20100−20130.
(12) Chinya, I.; Pal, A.; Sen, S. Flexible, hybrid nanogenerator based on Zinc Ferrite nanorods incorporated poly (vinylidene fluoride-co-hexafluoropropylene) nanocomposite for versatile mechanical energy harvesting. *Mater. Res. Bull.* **2019**, *118*, No. 110515.
(13) Chowdhury, A. R.; Abdullah, A. M.; Hussain, I.; Lopez, J.; Cantu, D.; Gupta, S. K.; Mao, Y.; Danti, S.; Uddin, M. J. Lithium doped zinc oxide based flexible piezoelectric-triboelectric hybrid nanogenerator. *Nano Energy* **2019**, *61*, 327−336.
(14) Si, S. K.; Karan, S. K.; Paria, S.; Maitra, A.; Das, A. K.; Bera, R.; Bera, A.; Halder, L.; Khatua, B. B. A strategy to develop an efficient piezoelectric nanogenerator through ZTO assisted γ-phase nucleation of PVDF in ZTO/PVDF nanocomposite for harvesting bio-mechanical energy and energy storage application. *Mater. Chem. Phys.* **2018**, *213*, 525−537.
(15) Silva, V. D.; Ferreira, L. S.; Simões, T. A.; Medeiros, E. S.; Macedo, D. A. 1D hollow MFe2O4 (M = Cu, Co, Ni) fibers by Solution Blow Spinning for oxygen evolution reaction. *J. Colloid Interface Sci.* **2019**, *540*, 59−65.
(16) Hu, P.; Yan, L.; Zhao, C.; Zhang, Y.; Niu, J. Double-layer structured PVDF nanocomposite film designed for flexible nano-generator exhibiting enhanced piezoelectric output and mechanical property. *Compos. Sci. Technol.* **2018**, *168*, 327−335.
(17) Eskandarloo, H.; Badiei, A.; Behnajady, M. A.; Tavakoli, A.; Ziarani, G. M. Ultrasonic-assisted synthesis of Ce doped cubic−hexagonal ZnTiO3 with highly efficient sonocatalytic activity. *Ultrason. Sonochem.* **2016**, *29*, 258−269.
(18) Sáaedi, A.; Yousefi, R.; Jamali-Sheini, F.; Cheraghizade, M.; Zak, A. K.; Huang, N. M. Optical and electrical properties of p-type Li-doped ZnO nanowires. *Superlattices Microstruct.* **2013**, *61*, 91−96.
(19) Chang, Y. T.; Chen, J. Y.; Yang, T. P.; Huang, C. W.; Chiu, C. H.; Yeh, P. H.; Wu, W. W. Excellent piezoelectric and electrical properties of lithium-doped ZnO nanowires for nanogenerator applications. *Nano Energy* **2014**, *8*, 291−296.
(20) Budigi, L.; Nasina, M. R.; Shaik, K.; Amaravadi, S. Structural and optical properties of zinc titanates synthesized by precipitation method. *J. Chem. Sci.* **2015**, *127*, 509−518.
(21) Xie, L.; Li, A.; Zhou, S.; Zhang, M.; Ding, Y.; Wang, P. Photocatalytic performance of nano-ZnTiO3 decorated with Ag/AgCl nanoparticles for degradation of the organic dyes. *Res. Chem. Intermed.* **2021**, *47*, 2373−2391.
(22) Bharti, D. K.; Gupta, M. K.; Kumar, R.; Sathish, N.; Srivastava, A. K. Non-centrosymmetric zinc silicate-graphene based transparent flexible piezoelectric nanogenerator. *Nano Energy* **2020**, *73*, No. 104821.
(23) Veeralingam, S.; Badhulika, S. Enhanced carrier separation assisted high-performance piezo-phototronic self-powered photo-detector based on core-shell ZnSnO3@ In2O3 heterojunction. *Nano Energy* **2022**, *98*, No. 107354.
(24) Wu, S.; Zhang, J.; Liu, X.; Lv, S.; Gao, R.; Cai, W.; Wang, F.; Fu, C. Micro-area ferroelectric, piezoelectric and conductive properties of single BiFeO3 nanowire by scanning probe microscopy. *Nanomaterials* **2019**, *9*, No. 190.
(25) Gruverman, A.; Kholkin, A.; Kingon, A.; Tokumoto, H. Asymmetric nanoscale switching in ferroelectric thin films by scanning force microscopy. *Appl. Phys. Lett.* **2001**, *78*, 2751−2753.
(26) Jiang, L.; Yang, P.; Fan, Y.; Zeng, S.; Wang, Z.; Pan, Z.; He, Y.; Xiong, J.; Zhang, X.; Hu, Y.; Gu, H.; et al. Ultrahigh piezoelectric coefficients of Li-doped (K, Na) NbO3 nanorod arrays with manipulated OT phase boundary: Towards energy harvesting and self-powered human movement monitoring. *Nano Energy* **2021**, *86*, No. 106072.
(27) Muduli, S. P.; Veeralingam, S.; Badhulika, S. Multilayered Piezoelectric Nanogenerator Based on Lead-Free Poly (vinylidene fluoride)-(0.67 BiFeO3-0.33 BaTiO3) Electrospun Nanofiber Mats for Fast Charging of Supercapacitors. *ACS Appl. Energy Mater.* **2022**, *5*, 2993−3003.
(28) Muduli, S. P.; Veeralingam, S.; Badhulika, S. Interface Induced High - Performance Piezoelectric Nanogenerator Based on a Electrospun Three-Phase Composite Nanofiber for Wearable Application. *ACS Appl. Energy Mater.* **2021**, *4*, 12593−12603.
(29) Veeralingam, S.; Gunasekaran, S. S.; Badhulika, S. Bifunctional NiFe LDH as a Piezoelectric Nanogenerator and Asymmetric Pseudo-capacitor. *Mater. Chem. Front.* **2022**, *6*, 2297−2308.
(30) Singh, H. H.; Khare, N. Flexible ZnO-PVDF/PTFE based piezo-tribo hybrid nanogenerator. *Nano Energy* **2018**, *51*, 216−222.
(31) Fang, L. S.; Tsai, C. Y.; Xu, M. H.; Wu, S. W.; Lo, W. C.; Lu, Y. H.; Fuh, Y. K. Hybrid nano-textured nanogenerator and self-powered sensor for on-skin triggered biomechanical motions. *Nanotechnology* **2020**, *31*, No. 155502.
(32) Shi, K.; Huang, X.; Sun, B.; Wu, Z.; He, J.; Jiang, P. Cellulose/BaTiO3 aerogel paper based flexible piezoelectric nanogenerators and the electric coupling with triboelectricity. *Nano Energy* **2019**, *57*, 450−458.
(33) Wang, X.; Yang, B.; Liu, J.; Zhu, Y.; Yang, C.; He, Q. A flexible triboelectric-piezoelectric hybrid nanogenerator based on P(VDF-TrFE) nanofibers and PDMS/MWCNT for wearable devices. *Sci. Rep.* **2016**, *6*, No. 36409.
(34) Suo, G.; Yu, Y.; Zhang, Z.; Wang, S.; Zhao, P.; Li, J.; Wang, X. Piezoelectric and triboelectric dual effects in mechanical-energy harvesting using BaTiO3/polydimethylsiloxane composite film. *ACS Appl. Mater. Interfaces* **2016**, *8*, 34335−34341.

https://doi.org/10.1021/acsanm.2c04731
ACS Appl. Nano Mater. 2023, 6, 1770−1782